Published in final edited form as:
Acad Radiol. 2009 May ; 16(5): 627–637. doi:10.1016/j.acra.2008.12.002.

Nanodelivery of MRI Contrast Agent Enhances Sensitivity of Detection of Lung Cancer Metastases

Matthew Freedman, M.D., MBA, **Esther H. Chang, Ph.D***, **Qi Zhou, MSc**, and **Kathleen F. Pirollo, Ph.D.**
Department of Oncology, Lombardi Comprehensive Cancer Center, Georgetown University Medical Center, Washington DC, 20057-1469

Abstract

Rationale and Objectives—Early detection of lung cancer can be problematic. While current imaging methods can identify lung cancers, they are limited in the size of nodules detectable.. There is also lack of evidence that these methods can correctly classify nodules <7 mm as malignant since lung cancer can be mimicked in appearance by benign lesions that lower specificity. Therefore, there is a need for enhanced sensitivity/specificity of detection for small lung cancers.

Materials and Methods—We have developed a nanosized (~100nm) immunolipsome complex for delivery of molecular medicines to tumors. In this complex an anti-transferrin receptor single-chain antibody fragment (TfRscFv) decorates the surface of a cationic liposome encapsulating the payload. We have previously shown that this systemically administered complex (scL) selectively targets, and efficiently delivers its payload into, tumor cells. We have also encapsulated MRI contrast agent gadopentetate dimegulamine ("gad-d") within this complex resulting in increased resolution and image intensity in a mouse model of primary cancer. Here we examine the ability of the scL-gad-d complex to increase the sensitivity of detection of lung metastases.

Results—These MRI studies show that the scL-gad-d nanocomplex is able to improve detection, and increase enhancement of, small lung cancers (400 microns and as small as 100 microns), when compared to that of uncomplexed gad-d.

Conclusions—Because of its tumor targeting specificity, deliver of an MRI contrast agent via this nanocomplex has potential for use as an agent that can identify small lung cancers, thus improving early detection and possibly increasing survival.

Keywords

Tumor-targeting; nanoimmunoliposome complex; early detection; lung cancer; enhanced MR imaging

INTRODUCTION

Lung cancer is the 2nd leading cause of cancer and the leading cause of cancer deaths for both men and women, with the number of cases in women on the rise. The American Cancer Society

*Corresponding Author: Esther H. Chang Ph.D., Professor, Department of Oncology, Lombardi Cancer Center TRB/E420, Georgetown University Medical Center, 3970 Reservoir Rd, NW, Washington, DC 20057-1469, Tel: (202) 687-8418, Fax: (202) 687-8434, Email: E-mail: change@georgetown.edu.

estimates that in 2008 there will be over 215,000 new cases of lung cancer in the US with more than 161,000 related deaths (1). The ratio of deaths to new cases (0.75) is significantly higher than the 0.4 ratio for cancer in general, indicating the dire prognosis of individuals who develop lung cancer and the importance of new approaches for early detection and diagnosis.

Currently the principal methods used for early identification of primary lung carcinoma are chest radiograph and chest computed tomography (CT). Although both methods are somewhat effective in identifying curable lung cancer (2–4), they possess a major drawback in that they commonly result in false positives, i.e. nodular areas that could indicate lung cancer, but are in fact due to scars or focal inflammatory/infectious processes (5–8). For small lung nodules this is a frequent occurrence and a serious problem. While there are various diagnostic methods to distinguish between true malignancies and false positives (9), for small lung nodules, the primary method is to obtain serial images over time to assess growth, a very inefficient, and costly process. Moreover, a recent report has associated the higher radiation dose from CT with an increased risk of cancer (10). Consequently, the need for multiple CT scans to confirm diagnosis may have a negative impact. There is also a risk entailed by delay in diagnosis. Cases with delays of 1 year have been associated with a change in stage (although delays of less than 6 months have not). This change in stage implies a worse prognosis (11–18). Furthermore, some small NSCLC can metastasize early (18).

In some cases contrast enhanced CT or MRI is used to determine the vascularity of the suspect area, although increased vascularity is not cancer specific. Moreover, a report by Bach, *et al* on the results of a multicenter trial concluded that lung CT may not meaningfully reduce the risk of advanced lung cancer or death (19). Thus, there is a pressing need for a new means of specifically identifying lung cancers at an early stage and predicting those nodules most likely to be malignant.

We have previously reported the use of an immunoliposome complex carrying contrast agent gadopentetate dimegulamine (“gad-d”) (Magnevist®, Berlex Laboratories, Wayne, N.J.) that enhanced MR Imaging of larger primary tumors in mouse models of cancer (20). This complex is a nano-sized construct of ~100nm in which the contrast agent is encapsulated in a cationic liposome (20). The surface of the liposome is decorated with an anti-transferrin receptor (TfR) single chain antibody fragment (TfRscFv) that serves to target the complex specifically and efficiently to tumor cells. This immunoliposome complex (scL) has also been used for systemic delivery of gene therapy to various types of tumors in mouse models including human pancreatic, breast, and mouse renal cell carcinomas (21–28). Our previous studies have shown the tumor-targeting specificity of this nanoimmunoliposome complex (21,23,24,27–29), clearly showing the enhanced uptake of the full complex as compared to that minus the targeting ligand both *in vitro* and *in vivo* (21,23,24,27–29). The use of this system to deliver wt p53 gene therapy is currently in Phase 1 clinical trials. By placing gad-d into this tumor specific immunoliposome complex, new and unique capabilities result from delivering MRI contrast media directly into tumor cells. This is accomplished via binding of the TfRscFv on the surface of the complex to the transferrin receptor (TfR) on the tumor cells with subsequent uptake of the gad-d bearing complex into the cell by receptor mediated endocytosis, an efficient process. Most tumor cells, including lung, prostate, ovarian, oral, colon, pancreatic, and breast cancer, express high levels of the transferrin receptor and have increased receptor recycling (30–35).

Here we assessed the ability of the complex to target and deliver the MR Imaging contrast agent gad-d to lung nodules in syngeneic mouse models of lung tumors. Our results show the requirement for the targeting ligand and demonstrate that scL-gad-d was able to target and deliver gad-d to lung nodules, as small as 100 microns in size. More significantly, we show the the enhancement of these lung nodules is greater with the scL-gad-d nanocomplex than with the uncomplexed (free) gad-d as currently used in the clinic.

METHODS

Cell lines

Mouse renal cell carcinoma cell line (RenCa) (36,37), was maintained in RPMI 1640 (Invitrogen, Carlsbad, CA) supplemented with 0.1mM non-essential amino acids (Invitrogen, Carlsbad, CA), 1mM sodium pryuvate (Invitrogen, Carlsbad, CA) 10% Fetal Bovine Serum (Quality Biological, Inc., Gaithersburg, MD), plus 2mM L-glutamine and 50mg/ml each of penicillin, streptomycin and neomycin (PSN).

Complex Formation

Cationic liposome (DOTAP:DOPE) was prepared by the ethanol injection method as previously described (24). The TfRscFv/Lip/gad-d complex (scL-gad-d) and the unliganded form of the complex (L-gad-d) (scL minus the TfRscFv tumor targeting moiety) were prepared as previously described (20).

Animal Models

Two different syngeneic mouse models of lung metastases were used in these studies. In the metastatic RenCa mouse model, 7.5×10^4 cells were intravenously tail vein injected in to 5–6 week old female BALB/c mice. For the small lung nodules (1–4 pixels, 100–400 microns in diameter) the animals were imaged 7–9 days post inoculation. For larger nodules the animals were imaged at 2–4 weeks post inoculation. In the B16/F10 mouse model, 1×10^5 cells were intravenously tail vein injected into 8–10 week old female C57Bl/6 mice. Two to three weeks post-inoculation the animals were used for imaging. All animal experiments were performed in accordance with and under approved Georgetown University GUACUC protocols.

Animal Imaging

The animal imaging was done with a 7T with a Bruker Biopsin (Billerica, MA, USA), using a respiratory gated (BioPac Physiological Data Monitor) T1-Weighted, 2 dimensional Turbo Multislice Multiecho imaging sequence. Animals to be imaged were anesthetized and placed in a proprietary, in-house designed, animal management system which incorporates a warm-water heating system that maintains the temperature at 37°C, as well as a four-channel, thermal optical monitoring system used to monitor animals' skin temperature, ambient temperature, and wall temperature of the device. For imaging, the animal was maintained under anesthesia with 1.5% isoflurane with a 66% oxygen and 30% nitrous oxide mixture. The anesthetized animal was positioned inside a cylindrical, variable RF resonant antenna (birdcage resonator volume coil) and tuned to a center frequency of approximately 300 MHz (the resonant frequency of water molecules when subject to a field strength of 7 T). The imaging parameters were: T1-Weighted 2D, TE 10.21 ms, TR400ms, Flipback off, 8 averages with a field of view of 2.56 × 2.56 cm and a 256 × 256 matrix. Depending on the size of the mouse, up to 22 slices were obtained with a usual slice thickness of 0.5 mm.

Pre-contrast injection images were obtained. After the baseline image was acquired, the animal was kept immobilized in the animal holder following which tail vein injections of free gad-d, L-gad-d or scL-gad-d, all at a dose of 5mg gad-d/20g mouse, were administered. Post injection imaging started within 90 seconds of the completion of injection. In each experimental comparison the amount of gad-d, uncomplexed or encapsulated within the liposome complex, was the same. For the small metastases, we determined that the pixel values of the nodules had returned to baseline within 24 hours. The injection sequence of gad-d or L-gad-d and scL-gad-d was varied with the alternate agent injected one to three days later. Image analysis was performed primarily with ImageJ Software (Wayne Rasband, National Institutes of Health, USA http://rsb.info.nih.gov/ij/)..

Statistics

Nodules were identified on the MRIs of 13 mice who received gad-d and 12 mice who received scL-gad-d. When combining the paired and unpaired studies, the p values were obtained using the Mann-Whitney U Test. Seven of the 13 mice were studied in a paired design using the Wilcoxon Matched Pairs Signed Ranks Test for analysis. One mouse was studied with and without TfRscFv targeting of the complex. For this descriptive statistics were used. All of the statistical analyses were done in SPSS (SPSS Inc. Chicago, IL)

RESULTS

Enhanced Contrast in a nodule 16 pixels in diameter with scL-gad-d

In Figure 1, we compared the pre-contrast images with the matched post-contrast studies for a 16 pixel in diameter (1.6 mm) RenCa nodule in the left lung (Figure 1A). While the pixel intensity increases from the baseline study of 6313 to 8034 (1721 units) with uncomplexed (free) gad-d, the increase was from 5413 to 10137 (4724 units) after i.v. injection of scL-gad-d. The change in pixel intensity, representing the level of enhancement for this lung nodule is shown in Figure 1B. The increase in pixel value is 2.7 times greater with scL-gad-d than with uncomplexed gad-d in this large lung nodule. Pleural metastases also showed increased enhancement with scL-gad-d.

Enhanced Contrast in nodules 4 pixels in diameter with scL-gad-d

Having determined that the scL-gad-d complex could bind to and enhance the imaging of the large lung nodules as compared to uncomplexed gad-d, we began to assess the limit of sensitivity of this approach by imaging progressively smaller RenCa lung tumors. These murine renal carcinoma cells, when i.v. inoculated, will reproducibly produce lung metastases. By decreasing the time between the cell injection and imaging, the sensitivity of detection of the scL-gad-d in progressively smaller lung nodules can be assessed.

In Figure 2A, two smaller nodules, ~4 pixels in size (400 micron), are identified. Although only the upper nodule can be visualized after free gad-d injection, both nodules are evident after injection of the scL-gad-d complex. Neither of the two nodules can be seen on the pre-contrast base studies. Where the nodules could not be seen, the expected location of the nodule was used for pixel value measurements. On the base (pre-contrast) view for the scL-gad-d, but not on the post contrast view, there was some atelectasis in the region of the upper nodule. Therefore, an area 1mm posterior to the visualized nodule was used for pixel values, since this was free from atelectasis.

The post-contrast pixel intensity of the upper nodule with free gad-d was 1857, while that with scL-gad-d complex was 2848, a difference of 991 units. For this upper nodule, the increase in intensity with contrast compared to the pre-contrast images is shown graphically in Figure 2B. The increase from the pre-contrast values was 2.1 times greater with scL-gad-d compared to free gad-d (1743 *vs* 844).

The lower nodule, with an intensity of 2938 was evident only after administration of scL-gad-d. While not detectable with free gad-d, the region where this nodule should be located measured 1121 post-injection, a value which corresponded closely to the pixel intensity of the pre-contrast images for both free gad-d and scL-gad-d. Thus, scL-gad results in greater enhancement than free gad-d of one small 4 pixel nodules and enables the visualization of an additional nodule not seen with free gad-d.

In the analysis of the images, we reviewed histograms of regions containing the nodule and pixel intensity profiles through the mid portion of the visible nodules. Figure 3 shows these

for the upper nodule and confirms its degree of enhancement and its diameter in pixels. Histograms of the regions of interest surrounding and including the upper lung nodule are given in Figure 3A. These histograms show that there are a group of pixels of higher value (near the peak of 2848) with the scL-gad-d than with uncomplexed gad-d (peak near 1857).

The corresponding profiles through the upper nodule at the center of the region of interest (ROI) with both free gad-d and scL-gad-d are shown in Figures 3B and 3C, respectively. The two profiles in each figure are one pixel apart in the superior/inferior axis. Both the pixel values (on the y-axis) and the number of adjacent pixels (on the x-axis) can be compared. The highest intensities in Figure 3B with free gad-d are 1609 and one just below 1609 in the left profile; while in the right profile the highest intensity is 1847. In comparison, when examining the profiles after injection of scL-gad-d (Figure 3C), the highest intensity in the left profile is 2662 with three pixels at approximately this value. The right profile has three pixels at or close to 2848.

Visualization of nodules 1–2 pixels in diameter by scL-gad-d

To determine the minimal nodule size detectable by the scL delivered gad-d, we imaged mice eight days after i.v. injection of the RenCa cells. In these studies free gad-d was not used since we were not able to visualize nodules less than 4 pixels in diameter with free gad-d (data not shown). One study revealed three extremely small lung nodules (Figure 4A). The two smaller nodules (N1 and N2) measure 1–2 pixels in size on the MR images (full width at half max in the profiles) and thus are approximately 100–200 microns.

The changes in pixel value of these three small nodules are graphically represented in Figure 4B. Nodules 1 and 2 could not be identified on the pre-contrast images. As a control we also measured an area on the same slice where no nodule could be identified either without or with scL-gad-d. The pre-contrast values at the locations of the nodules are all approximately the same (Figure 4B) and are slightly (but not significantly) higher than the nodule free area used for comparison. Post contrast, minimal enhancement is shown in the area with no nodule. However, for all three nodules the change in pixel intensity (the difference between baseline/pre-contrast values and post-contrast values) from the pre-contrast values is 2.6, 4.8 and 6.6 fold greater with the scL-gad-d complex than the difference observed pre and post-contrast in the nodule-free lung parenchyma (1518 to 1663).

A histogram (Figure 5A) of the region of the 100 micron Nodule 1 indicates that there is only one outlier pixel and that either this enhances with scL-gad-d or a new pixel has increased sufficiently to be identified on the image. The Y-axis on the left chart is 3 pixels maximum, while that on the right chart is 2 pixels maximum. The profile, drawn through the mid portion of Nodule 1 (Figure 5B), shows that only a single pixel reaches the intensity of 1946 seen on the histogram in Figure 5A.

Similar analysis post contrast with scL-gad-d was performed on Nodules 2 and 3 from Figure 4A. The histograms and profiles through the center of these nodules are shown in Figures 6A and B, respectively. The histogram for the larger Nodule 3 shows that there are two pixels close to 2542 (solid edged oval), with three pixels nearby (dotted edged oval) (Figure 6B). The profile through the center of the nodule shows that there are two pixels that are close to 2542 (pixel intensity 2532, 2475) and three that are near, but with lower intensity (pixel intensity 2254, 2254, 2187). The diameter of this nodule is 4 pixels, approximately 400 microns, estimating full width at half max from the profile.

A summary of the increase in pixel intensity with scl-gad-d of the two small (1–2 pixel, 100–200 micron) metastatic lung nodules (Nodules 1 and 2) and the 4 pixel Nodule 3 shown in Figure 4A is given in Table 1. This Table indicates the mean, standard deviation (SD), and

maximum pixel intensity of the nodules. For each nodule it also gives the Z-score of the maximum pixel value and the expected frequency of pixels at or above this Z-score. The increase in maximum pixel intensity for Nodule 1 is 1.1 SD, for Nodule 2 it is 2.3 SD, and for Nodule 3 it is 3.4 SD above the pre-contrast SD of the mean for the respective nodule. For Nodules 2 and 3, this increase is statistically significant ($p < 0.02$)

Histology Studies

To confirm that the extremely small images seen with scL-gad-d on MRI Figure 4A were in fact tumor nodules, after completion of the MRI, H&E stained sections through the lobe of the lung where the nodules were observed by MRI were examined. The results are shown in Figure 7. Two renal cell metastases (arrows) were identified. These two small metastases correspond to the approximate location of the nodules identified post-contrast with scL-gad-d by MRI and measure < 100 microns in size. They are also approximately 650 microns apart. These histology findings are similar to the prospective measurements on the MRI of two 100–200 micron nodules separated by approximately 700 microns. Other serial sections show that the second tumor is attached to the lung and is not a free fragment (data not shown). No other small tumor nodules were observed in any of the sections examined.

Comparison between targeted and untargeted complex

To demonstrate the importance of the targeting molecule, MRI contrast enhancement in the same mouse was compared between scL-gad-d and the complex minus the TfRscFv molecule (L-gad-d). Two small nodules could be matched between the studies. The first nodule increased from 4436 to 4503 pixel intensity units with the non-targeted L-gad-d (Figure 8A), and from 2201 to 3998 units with the targeted scL-gad-d (Figure 8B). This represents an increase of 67 compared to 1797 pixel units over baseline values, for L-gad-d and scL-gad-d, respectively. For the second nodule (not shown), the L-gad-d resulted in an increase from 3996 to 4164 pixel intensity units (an increase of 168 units over baseline values) and while the scL-gad-d increased from 2155 to 2893 pixel intensity units (an increase of 738 units over baseline value). The increase for both nodules is presented graphically in Figure 8C. Thus for both lung nodules there is greater enhancement with scL-gad-d compared to that seen with L-gad-d.

DISCUSSION

Worldwide, it is estimated that lung cancer causes nearly one million deaths annually (38). Overall, in the United States, 90% of the 190,000 new cases (86% of which are non-small cell (NSCLC) will die within two years (38,39), However, for pathologic stages 1A and 1B, the five year survival is much greater (67% and 57%, respectively) (40).

Chest X-Ray and lung CT are the most common methods of lung cancer detection. With both, a major problem is due to findings that could represent cancer, but that, on further evaluation, are actually benign. These are usually considered to be “false positives.” In lung CT screening, the false positive rate for all lung nodules is as high as 96% (8). For example, the report of the prevalence screen from the PLCO, indicates that among the 5991 radiographs suspicious for lung cancer all but 206 were shown to not have cancer prior to biopsy. Of the remaining 206 cases that were biopsied, only 61% actually had lung cancer (38). Thus, only 126 cases were identified with cancer from the 5991 positive suspicious radiographs, or only about 2% of the total. Additionally, in a recent report of 5 years of CT screening (8), only 68 lung cancers were present among the 3359 non-calcified nodules that were identified by CT. The remaining 98% were false positives.

Assessment of possible malignancy can be based on lack of change from prior studies, structural features of nodules, their size, growth over time and patterns of contrast

enhancement. Contrast enhanced Contrast enhanced CT imaging of nodules for assessment of vascularity has high sensitivity, but only medium specificity, for the diagnosis of cancerous nodules greater than 7 mm, (41–47). It is less effective for smaller nodules. We estimate that a 7 mm nodule would likely be 10 or more pixels in diameter. However, at least 44% of CT detected lung nodules are less than 4 mm (8). Thus, there is a serious need for increased specificity of diagnosis, and techniques that can correctly classify these smaller nodules would have significant clinical impact.

The studies described above were performed to assess if the scL-gad-d targeted to the TfR would show greater enhancement than the non-targeted complex, and the non-complexed (free) gad-d.. Once this was demonstrated (Figure 1), studies continued to determine the smallest lung metastases in which contrast uptake could be identified. Pixel intensity was used to compare 1) pre-contrast to contrast enhanced images, 2) TfR targeted and non-targeted contrast, and (3) free gad-d to scL-gad-d. Although pixel intensity is not in linear relationship to the concentration of gadolinium based contrast agents, in the contrast ranges used, a higher pixel value does represent a greater accumulation of contrast media (20). We were able to show MR enhancement of nodules in mice as small as 1–2 pixels in diameter (0.1 to 0.2mm). This would translate to a nodule of approximately 0.7–1.4mm in humans, significantly smaller than those reported to enhance with contrast by CT. Unlike standard CT contrast, scL-gad-d targets and is actively taken up into cancer cells (20); higher uptake and longer persistence of contrast in the nodule via the scL delivery system should increase the likelihood of classifying a nodule as a malignancy. Thus this approach would allow most benign nodules to be differentiated from potentially malignant nodules at a size approximately 5 times smaller than shown with current contrast enhanced CT.

To control for the possibility that image noise was simulating nodules 1–3 pixels in size several techniques of analysis were combined. First, the small nodule must be visible to the human observer at least on the post contrast image. Second, the histogram of a small region surrounding the nodule should show that the peak intensity was more than two standard deviations above the mean. Third, a two-dimensional profile through the visible nodule should show the same peak pixel values as those demonstrated on the histogram. Fourth, for nodules two or more pixels in size, these high value pixels should be shown to be contiguous on the profile. Last, the nodule size detected by imaging should be consistent with the nodule size measured on histology, matching the region of imaging and histology as closely as feasible. Because the RenCa model can reproducibly produce lung metastases, the size of the nodules is quite uniform even when small (36–37).

We showed that enhancement was, on average, greater with the scL-gad-d, $p < 0.02$ (Mann-Whitney U Test). In total, seven mice were studied in a paired design. Of these, contrast enhancement was greater with scL-gad-d in 6, and less in 1 ($p < 0.05$ by Wilcoxon Matched Pairs Signed Ranks Test).

The nodule identified in Fig 4A which was determined to be approximately 4 pixels in diameter, appears larger in the MR image when enhanced by scL-gad-d compared to free gad-d. The histograms demonstrate a greater number of pixels at the upper end of the histograms for scL-gad-d. With free gad-d, two pixels, almost superimposed on the histogram, are at the maximum level. In contrast with scL-gad-d there are at least four pixels, and more likely eight pixels that are enhanced when two profiles one pixel away are included. Thus, with scL-gad-d the nodule appears on the image visibly larger and the change in histogram supports this interpretion. The pixel values (x-axis on the two charts) indicate a higher degree of pixel intensity with scL-gad-d than with gad-d. For free gad-d, the high pixel is 2.8 SD above the mean. For scL-gad-d, the high pixel is 1.9 SD above the mean. This suggests that these outlying pixels are consistent with small nodules, rather than representing random variation in pixel intensity, particularly

given the small number of pixels in each measured region of interest. These data demonstrate that small nodules of 4 pixels (~0.4 mm) are more greatly enhanced by encapsulating the gad-d contrast agent in the scL nanocomplex.

We have also demonstrated the ability of gad-d, when encapsulated in the scL complex to enhance lung nodules as small as 1–2 pixels in diameter. Histogram analysis (Fig. 5) of the small nodules in Fig 4A show that for Nodule 1, the peak pixel value pre-contrast is 2.9 SD above the mean, while the peak measurement post contrast is 3.3 SD above the mean. In addition, the extremely small (0.1mm) Nodule 2 in Fig. 4A also showed only a single pixel reaching peak value, which was 4.0 SD above the mean (Figure 6A). For the larger Nodule 3, the peak pixel value was 2.3 SD above the mean. These data indicate that it is unlikely that the highest pixel value is due to random noise variation, but represents a nodule that likely shows some enhancement. Furthermore, while there was significant enhancement of the small nodules after injection of scL-gad-d the fact that there was only minimal enhancement in the nodule free parenchyma, as shown in Figure 4B, also demonstrates that the enhancement seen with the scL-gad-d is tumor tissue specific.

A summary of the increase in pixel intensity with scL-gad-d of the two small (1–2 pixel, 100–200 micron) metastatic lung Nodules (Nodules 1 and 2) and the 4 pixel Nodule 3 shown in Figure 4A is given in Table 1. This Table indicates the mean, standard deviation (SD), and maximum pixel intensity of the nodules. For each nodule imaged it also gives the Z-score of the maximum pixel value and the expected frequency of pixels at or above this Z-score. From this table, one can see that the pixel intensity of these small nodules is unlikely to be due to random noise. In addition, one can see the increase in pixel intensity comparing scL-gad-d to the pre-contrast image. The method used to identify very small lung nodules is based on statistical image processing. This is a method adapted from the field of astronomy which has previously been applied in pilot studies in digital mammography (48). The approach is based on identifying statistical outliers, 3 or more standard deviations (SD) above the mean, i.e. Z-score $\geq$ 3.0. The histogram data for the lung MRIs used in this experiment is basically Gaussian with outlying pixels seen at the upper portion of the histogram (data not shown). For a Z-score of 3, one would expect 1.4 pixels per 1000 above this cut point. For a Z-score of 4, one would expect 3.2 per 100,000. When we measure the pixel intensity of the very small nodules identified on the images, these have the Z-scores shown in Table 1. Thus, it is unlikely, given the number of pixels included in the analysis of nodules and their surroundings that the pixels we assign as representing nodules represent noise. When the same area can be seen on two studies (pre-contrast and post contrast) or with two conditions (gad-d and scL-gad-d) the likelihood of this occurring by chance is even less.

Although it is difficult to definitely distinguish image noise from very small lung nodules. In this case, we have presented evidence that the small nodules we are detecting (1) consist of pixel intensity value outliers, 2–4 SD from the mean, (2) that the area of suspected nodule does enhance, whereas areas with no visible nodule enhance minimally, (3) that the same outlier pattern we see with nodules 2–4 pixels in size is seen with the 1–2 pixel nodules, and (4) we have provided histologic confirmation of nodule size and the distance separating two identified nodules for this case where histology was obtained after carefully aligning the location for histology with the identified location on the MRI. Therefore, based on histology and the care we used to align the histology to the MRI, we believe that we have likely shown enhancement in 100 micron metastases to the lung when gad-d is delivered to the tumors by the targeted scL nanocomplex.

Thus, the data presented here suggests strongly that the use of scL-gad-d has the potential to enable physicians to rapidly identify almost all of the cases that represent cancer through

improvements in contrast enhancement of the lung nodules. Moreover, this approach could also be used to identify small metastases in other places throughout the body.

CONCLUSIONS

The research reported here shows that a novel nano-sized tumor-targeting immunoliposome complex carrying gad-d can successful enhance very small lung nodules 2–4 pixels in size and even nodules only 1 pixel in size. The next step will be to apply this to a mouse model of primary lung adenocarcinoma and models of small nodular scars in the lungs. Because of the tumor-targeting nature of the complex we envision that this approach may also be able to distinguish malignant nodules from the many small benign scars identified in the lungs on CT. We are actively developing this nanotechnology as a clinically useful agent to improve early detection of lung cancer.

Acknowledgments

Financial Support: This work was supported in part by STTR Phase I grant 1R41 CA 121453-01 (E.H.C. M.F. and K.F.P), and a research grant from SynerGene Therapeutics (K.F.P). These studies were conducted in part using the Histopathology and Tissue, and Animal Core Facilities supported by NCI Cancer Center Support grant and USPHS grant 2P30-CA-51008 and 1 S10 RR 15768-01. This investigation was conducted in part in a facility constructed with support from Research Facilities Improvement grant C06RR14567 from the National Center for Research Resources, NIH.

We wish to thank Dr. Stanley T. Fricke, Ms. Lilia Ileva, and Mr. Ayichew Hailu for their kind assistance with the acquisition of the MR images.

References

1. American Cancer Society. Cancer Facts and Figures 2008. http://www.cancer.org
2. Gohagan J, Marcus P, Fagerstrom R, et al. Writing Committee LSSRG. Baseline findings of a randomized feasibility trial of lung cancer screening with spiral CT scan vs chest radiograph: the Lung Screening Study of the National Cancer Institute. Chest 2004;126:114–121. [PubMed: 15249451]
3. Gohagan JK, Marcus PM, Fagerstrom RM, et al. Final results of the Lung Screening Study, a randomized feasibility study of spiral CT versus chest X-ray screening for lung cancer. Lung Cancer 2005;47:9–15. [PubMed: 15603850]
4. Henschke CI, Yankelevitz DF, et al. International Early Lung Cancer Action Program. Survival of patients with stage I lung cancer detected on CT screening. New England Journal of Medicine 2006;355:1763–1771. [PubMed: 17065637]
5. Stitik FP, Tockman MS. Radiographic screening in the early detection of lung cancer. Radiologic Clinics of North America 1978;16:347–366. [PubMed: 746141]
6. Stitik, FP.; Tockman, MS.; Khouri, N. Chest Radiology. In: Miller, AB., editor. Screening for Cancer. New York: Academic Press; 1985. p. 163-191.
7. Swensen SJ, Jett JR, Hartman TE, et al. Lung cancer screening with CT: Mayo Clinic experience. Radiology 2003;226:756–761. [PubMed: 12601181]
8. Swensen SJ, Jett JR, Hartman TE, et al. CT screening for lung cancer: five-year prospective experience. Radiology 2005;235:259–265. [PubMed: 15695622]
9. Pinsky PF, Marcus PM, Kramer BS, et al. Diagnostic procedures after a positive spiral computed tomography lung carcinoma screen. Cancer 2005;103:157–163. [PubMed: 15529306]
10. Brenner DJ, Hall EJ. Computed tomography- an increasing source of radiation exposure. New England Journal of Medicine 2007;357:2277–2284. [PubMed: 18046031]
11. Bozcuk H, Martin C. Does treatment delay affect survival in non-small cell lung cancer? A retrospective analysis from a single UK centre. Lung Cancer 2001;34:243–252. [PubMed: 11679183]
12. Pita-Fernandez S, Montero-Martinez C, Pertega-Diaz S, et al. Relationship between delayed diagnosis and the degree of invasion and survival in lung cancer. Journal of Clinical Epidemiology 2003;56:820–825. [PubMed: 14505765]

13. Quarterman RL, McMillan A, Ratcliffe MB, et al. Effect of preoperative delay on prognosis for patients with early stage non-small cell lung cancer. [see comment]. Journal of Thoracic & Cardiovascular Surgery 2003;125:108–113. [PubMed: 12538992]

14. Kashiwabara K, Koshi S, Itonaga K, et al. Outcome in patients with lung cancer found on lung cancer mass screening roentgenograms, but who did not subsequently consult a doctor. Lung Cancer 2003;40:67–72. [PubMed: 12660008]

15. Yoshimoto A, Tsuji H, Takazakura E, et al. Reasons for the delays in the definitive diagnosis of lung cancer for more than one year from the recognition of abnormal chest shadows. Internal Medicine 2002;41:95–102. [PubMed: 11868615]

16. Aragoneses FG, Moreno N, Leon P, et al. Influence of delays on survival in the surgical treatment of bronchogenic carcinoma. Lung Cancer 2002;36(1):59–63. [PubMed: 11891034]

17. Myrdal G, Lambe M, Hillerdal G, et al. Effect of delays on prognosis in patients with non-small cell lung cancer. Thorax 2004;59(1):45–49. [PubMed: 14694247]

18. Tammemagi M, Freedman MT, Oken M, et al. Factors associated with human small aggressive non-small cell lung cancer. Cancer Epidemiology Biomarkers & Prevention 2007;16(10):2082–2089.

19. Bach PB, Jett JR, Pastorino U, et al. Computed tomography screening and lung cancer outcomes. JAMA 2007;297:953–961. [PubMed: 17341709]

20. Pirollo KF, Dagata J, Wang P, et al. A tumor-targeted nanodelivery system to improve early MRI detection of cancer. Molecular Imaging: Official Journal of the Society for Molecular Imaging 2006;5:41–52. [PubMed: 16779969]

21. Xu L, Pirollo K, Tang W-H, et al. Transferrin-liposome-mediated systemic p53 gene therapy in combination with radiation results in regression of human head and neck cancer xenografts. Human Gene Therapy 1999;10:2941–2952. [PubMed: 10609655]

22. Xu L, Pirollo K, Rait A, et al. Systemic p53 gene therapy in combination with radiation results in human tumor regression. Tumor Targeting 1999;4:92–104.

23. Xu L, Tang W, Huang C, et al. Anti-transferrin Receptor ScFv-Targeted Immunolipoplexes for Systemic Cancer Gene Therapy. Molecular Medicine 2001;10:723–734. [PubMed: 11713371]

24. Xu L, Huang C-C, Huang W-Q, et al. Systemic Tumor-targeted Gene Delivery by Anti-Transferrin Receptor scFv-Immunoliposomes. Molecular Cancer Therapeutics 2002;1:337–346. [PubMed: 12489850]

25. Rait AS, Pirollo KF, Xiang L, et al. Tumor-targeting, systemically delivered antisense HER-2 chemosensitizes human breast cancer xenografts irresective of HER-2 levels. Molecular Medicine 2002;8:475–486. [PubMed: 12435858]

26. Rait AS, Pirollo KF, Ulick D, et al. HER-2-targeted antisense oligonucleotide results in sensitization of head and neck cancer cells to chemotherapeutic agents. Annals of the New York Academy of Sciences 2003;1002:78–89. [PubMed: 14751825]

27. Pirollo KF, Zon G, Rait A, et al. Tumor-targeting nanoimmunoliposome complex for short interfering RNA delivery. Human Gene Therapy 2006;17:117–124. [PubMed: 16409130]

28. Pirollo KF, Rait A, Zhou Q, et al. Materializing the potential of small interfering RNA via a tumor-targeting nanodelivery system. Cancer Research 2007;67:2938–2943. [PubMed: 17409398]

29. Yu W, Pirollo KF, Yu B, et al. Enhanced transfection efficiency of a systemically delivered tumor-targeting immunolipoplex by inclusion of a pH-sensitive histidylated oligolysine peptide. Nucleic Acids Research 2004;32:e48. [PubMed: 15026537]

30. Keer HN, Kozlowski JM, Tsai YC, et al. Elevated transferrin receptor content in human prostate cancer cell lines assessed in vitro and in vivo. Journal of Urology 1990;143:381–385. [PubMed: 1688956]

31. Rossi MC, Zetter BR. Selective stimulation of prostatic carcinoma cell proliferation by transferrin. Proceedings of the National Academy of Sciences of the United States of America 1992;89:6197–6201. [PubMed: 1631108]

32. Elliott RL, Elliott MC, Wang F, et al. Breast carcinoma and the role of iron metabolism. a cytochemical, tissue culture, and ultrastructural study. Ann N Y Acad Sci 1993;698:159–166. [PubMed: 8279755]

33. Thorstensen K, Romslo I. The transferrin receptor: its diagnostic value and its potential as therapeutic target. Scandinavian Journal of Clinical & Laboratory Investigation - Supplement 1993;215:113–120. [PubMed: 8327847]
34. Miyamoto T, Tanaka N, Eishi Y, et al. Transferrin receptor in oral tumors. International Journal of Oral & Maxillofacial Surgery 1994;23:430–433. [PubMed: 7890992]
35. Whitney JF, Clark JM, Griffin TW, et al. Transferrin receptor expression in nonsmall cell lung cancer. Histopathologic and clinical correlates 1995;76(1):20–25.
36. Chakrabarty A, Hillman GG, Maughan RL, et al. Influence of tumor site on the therapy of murine kidney cancer. Anticancer Research 1994;14:373–378. [PubMed: 8017836]
37. Salup RR, Herberman RB, Chirigos MA, et al. Therapy of peritoneal murine cancer with biological response modifiers. Journal of Immunopharmacology 1985;7:417–436. [PubMed: 3878855]
38. Oken MM, Marcus PM, Hu P, et al. Baseline chest radiograph for lung cancer detection in the randomized Prostate, Lung, Colorectal and Ovarion Cancer Screening Trial. Journal of the National Cancer Institute 2005;97(24):1832–1839. [PubMed: 16368945]
39. Centers for Disease Control and Prevention (CDC). Recent trends in mortality rates for four major cancers, by sex and race/ethnicity--United States, 1990–1998. MMWR -Morbidity & Mortality Weekly Report 2002;51:49–53. [PubMed: 11843259]
40. Mountain CF. Revisions in the International System for Staging Lung Cancer. Chest 1997;111:1710–1717. [PubMed: 9187198]
41. Swensen SJ. Functional CT: lung nodule evaluation. Radiographics 2000;20:1178–1181. [PubMed: 10903707]
42. Swensen SJ, Viggiano RW, Midthun DE, et al. Lung nodule enhancement at CT: multicenter study. Radiology 2000;214:73–80. [PubMed: 10644104]
43. Swensen SJ, Brown LR, Colby TV, et al. Pulmonary nodules: CT evaluation of enhancement with iodinated contrast material. Radiology 1995;194:393–398. [PubMed: 7824716]
44. Swensen SJ, Brown LR, Colby TV, et al. Lung nodule enhancement at CT: prospective findings. Radiology 1996;201:447–455. [PubMed: 8888239]
45. Jeong YJ, Lee KS, Jeong SY, et al. Solitary pulmonary nodule: characterization with combined wash-in and washout features at dynamic multi-detector row CT. Radiology 2005;237:675–683. [PubMed: 16244276]
46. Zhang M, Kono M. Solitary pulmonary nodules: evaluation of blood flow patterns with dynamic CT. Radiology 1997;205:471–478. [PubMed: 9356631]
47. Maki DD, Gefter WB, Alavi A. Recent advances in pulmonary imaging. Chest 1999;116:1388–1402. [PubMed: 10559104]
48. Page D. The strange courtship of astronomy and mammography. Digital Imaging Magazine. December;1995

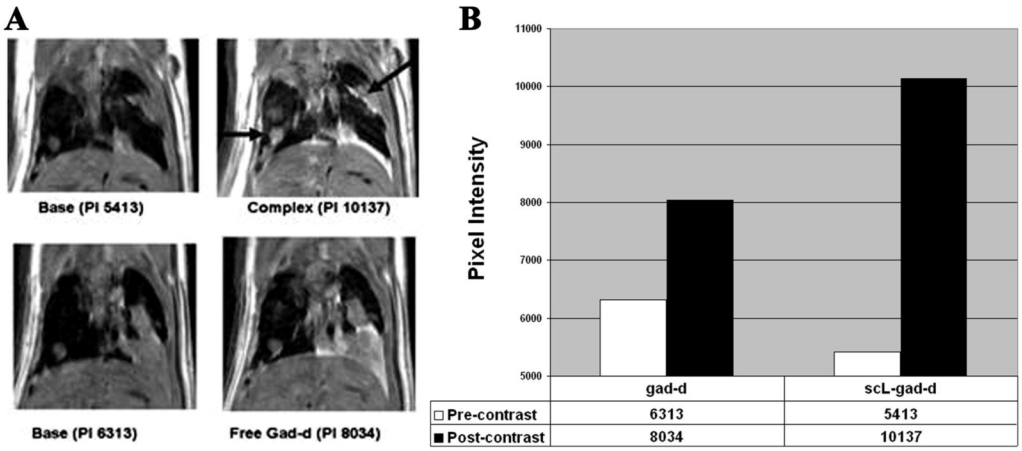

Figure 1. Metastases to lung in the RenCa lung metastasis model

In this composite figure/chart, we compare the image of the same mouse imaged with both free gad-d and scL-gad-d. **A**-The base views show the respective pre-contrast images. **PI** = pixel intensity of the lower left lung nodule. **B**-This is graphically shown in the Chart that shows the enhancement from the precontrast images. The scL-gad-d complex shows greater enhancement than free gad-d in this metastasis. Arrows indicate the nodule measured and the enhancing pleural metastases.

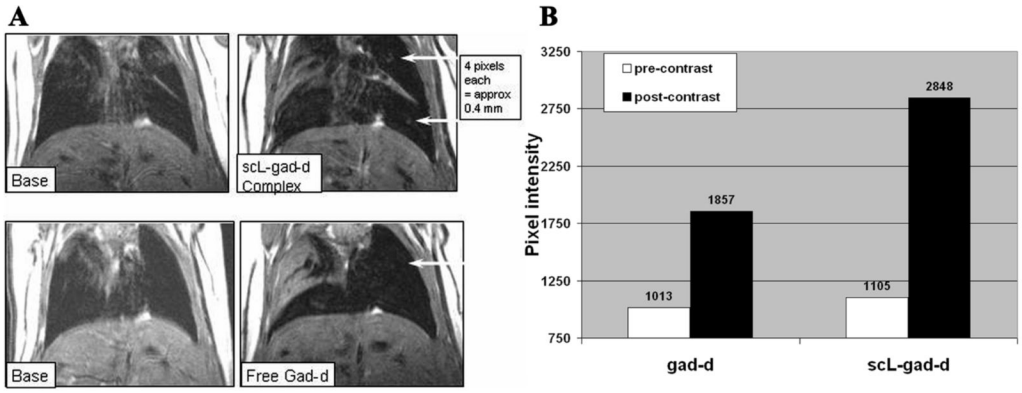

Figure 2. Detection of 4 pixel RenCa nodules

A- Pixel Intensity of upper nodule with free gad-d was 1857, while that with scL-gad-d complex was 2848. This upper nodule does not show on base (pre-contrast image) with free gad-d and either does not show or is hidden in atelectasis on base for complex. The lower nodule is not visible except with complex. Its intensity is 2938. The region of the nodule measures 1121 with free gad-d, but the nodule itself cannot be identified. **B**-This chart demonstrates the increase in peak pixel intensity in the region including the small (approximately 4 pixel—400 micron) upper lung nodule shown in **A**

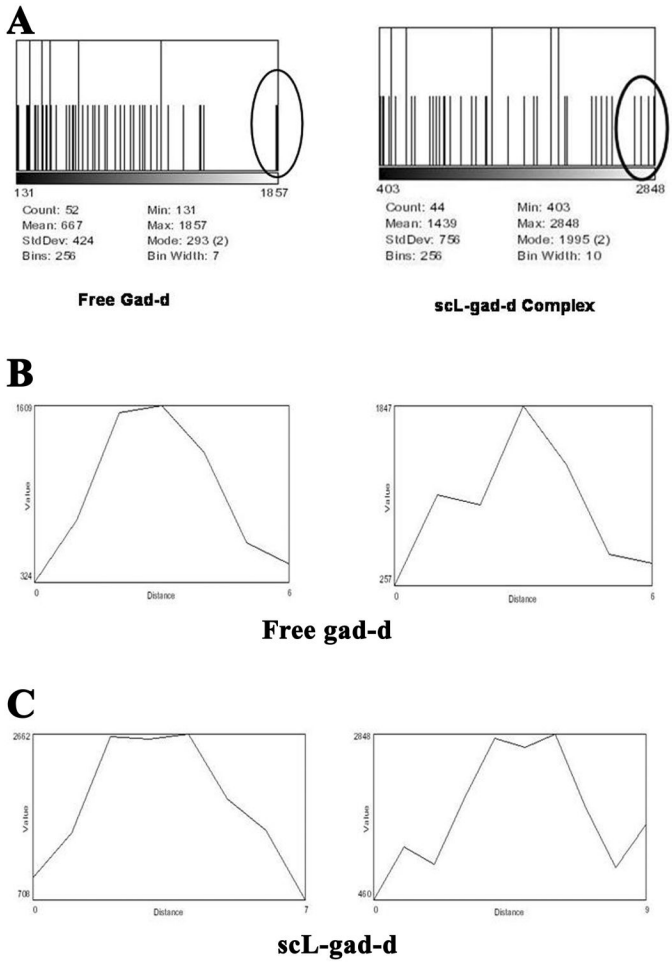

Figure 3. Histograms corresponding to the RenCa nodules in Figure 2

A-These histograms of the region of the nodule display the spread of pixel intensities (x-axis) vs the number of pixels of that value (y-axis). The maximum y-axis for these images is 2 pixels. The histogram charts provide both the mean and standard deviation levels. **B**- Standard gad-d: Two profiles, one pixel apart, through the center of the upper nodule after enhancement with gad-d. **C**- scL-gad-d. Two profiles, one pixel apart, through the center of the upper nodule after enhancement with scL-gad-d.

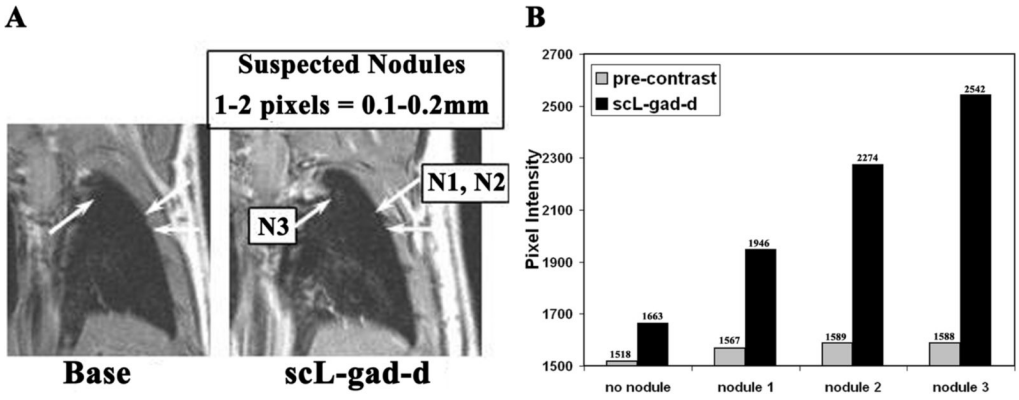

Figure 4. Detection of 1–2 pixel RenCa lung metastases

A-Three lung nodules are identified on the post contrast scL-gad-d images. The two smaller nodules (N1 and N2) measure 1–2 pixels (approximately 100–200 microns) in size. They measure about 700 microns apart. They are just barely visible on the pre-contrast images. The Arrows indicate the lung nodules. **B**- Chart showing the change in pixel value of the three small nodules identified in Figure 4A.

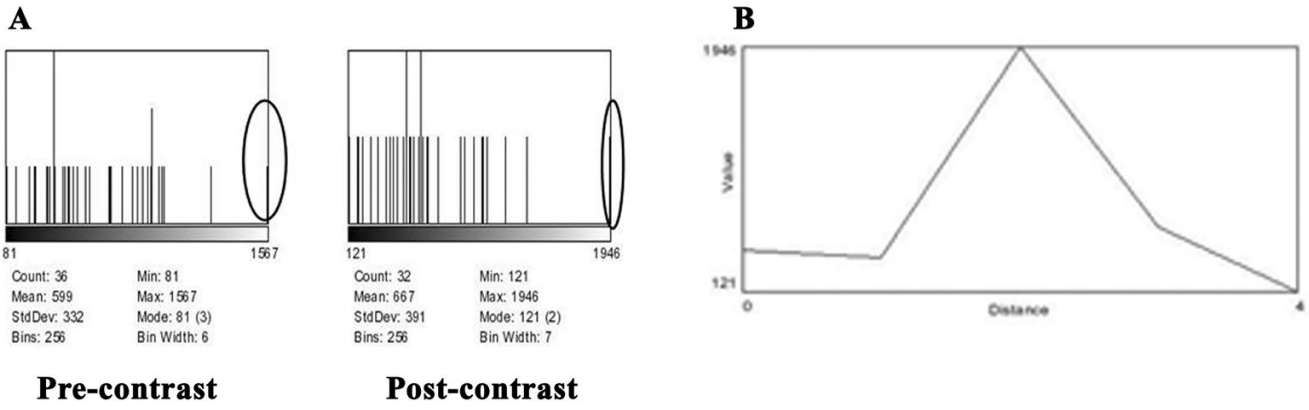

Figure 5. Nodule 1 from Figure 4A, pre and post contrast with scL-gad-d

A- Histogram of pre and post- contrast with scL-gad-d. **B**-Profile through Nodule 1

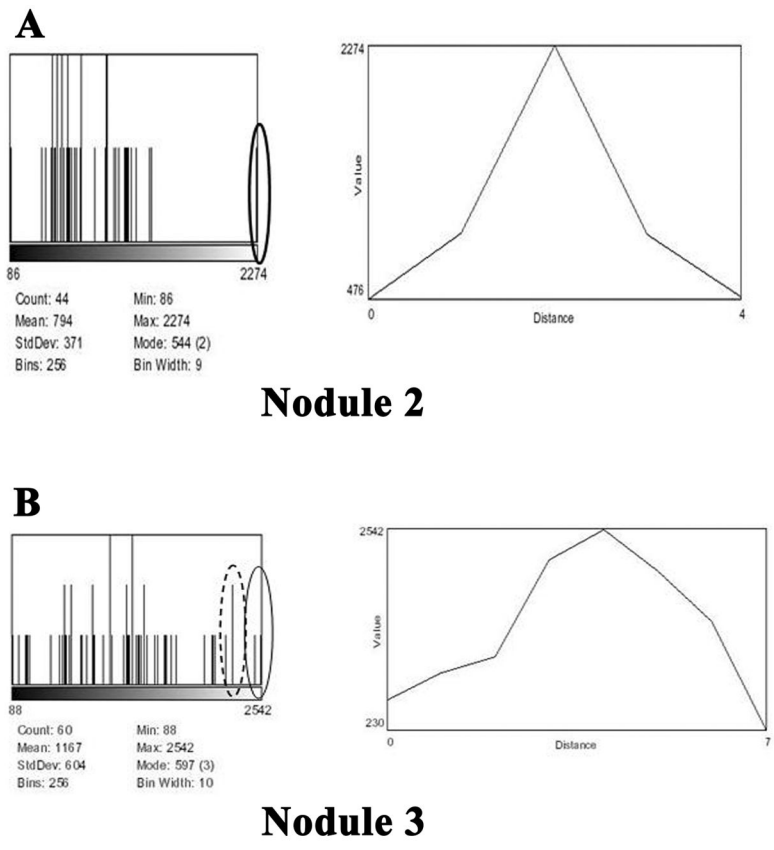

Figure 6. Data for Nodules 2 and 3 from Figure 4A post contrast with scL-gad-d with histogram and profile through the center of the nodule

A-Histogram and profile for Nodule 2. **B**-Histogram and profile for Nodule 3.

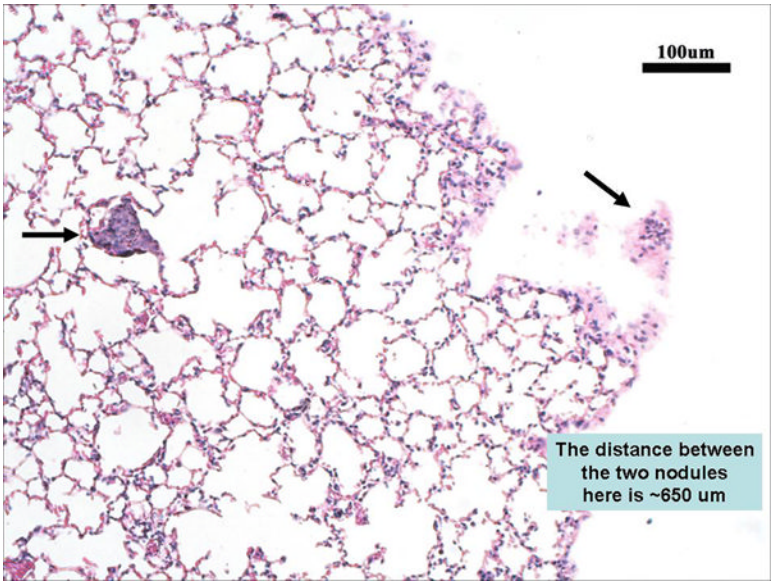

Figure 7. Histology section (H&E stain) of the lungs from the mouse described above (Figure 4A)
MR images were used to guide the sectioning of the lungs. Arrows point to the two small metastases, each less than 100 microns in size.

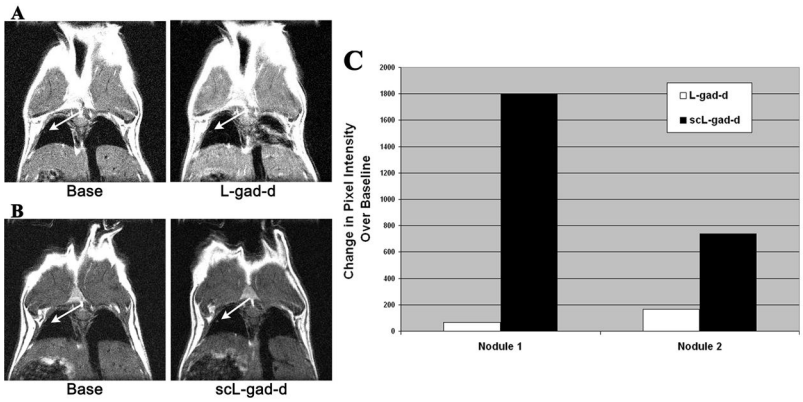

Figure 8. Comparison of MR image enhancement between targeted and unliganded complex

In this composite figure/chart, we compare the image of the same mouse imaged with both scL-gad-d and unliganded gad-d (L-gad-d). **A**-The base view and post-contrast image after i.v. injection of the unliganded L-gad-d. **B**- The base view and post-contrast image after i.v. injection of the targeted scL-gad-d. **C**- A graph of the enhancement over baseline values with both agents.

Table 1

This table lists the pixel intensities of the three nodules shown in Figure 4A. Mean, SD, Maximum, and Z-scores are given. The Z-scores show that the maximum pixel intensity in the location of the visualized nodules is always at least 2.9 SD above the mean, indicating that the presumed 1–4 pixel nodules are not likely to be due to image noise.

		MEAN	SD	Maximum	Z-Score	Expected pixel frequency at and above this Z -score
Nodule 1	Pre-contrast	599	332	1567	2.92	4 per 1000
	Post scL-gad-d	667	391	1946	3.27	5 per 10,000
Nodule 2	Pre-contrast	591	299	1589	3.34	4 per 10,000
	Post scL-gad-d	665	339	2274	4.75	1 per 100,000
Nodule 3	Pre-contrast	566	278	1588	3.68	1 per 10,000
	Post scL-gad-d	981	515	2542	3.03	1 per 1000